JOURNAL OF GEOPHYSICAL RESEARCH, VOL. 115, B06320, doi:10.1029/2009JB006960, 2010

Energetics of strain localization in a model of seismic slip

A. M. Hermundstad,[1] E. G. Daub,[1,2] and J. M. Carlson[1]

Received 7 September 2009; revised 11 December 2009; accepted 20 January 2010; published 29 June 2010.

[1] We quantify the energy dissipated to heat and to local disorder in a sheared layer of granular fault gouge. Local disorder is modeled using shear transformation zone theory, a continuum model of nonaffine deformation in amorphous solids that resolves spontaneous localization of strain. Strain localization decreases the total energy dissipated during slip. In addition, a fraction of this energy is dissipated to increasing local disorder as the material is sheared, thereby decreasing the amount of energy dissipated as thermal heat. We quantify the heat dissipated per unit area as a function of total slip in the presence and absence of strain localization and test the parameter dependence of these calculations. We find that less heat is dissipated per unit area compared to results obtained using a traditional heuristic energy partition.

Citation: Hermundstad, A. M., E. G. Daub, and J. M. Carlson (2010), Energetics of strain localization in a model of seismic slip, *J. Geophys. Res.*, *115*, B06320, doi:10.1029/2009JB006960.

1. Introduction

[2] Developing quantitative methods for partitioning released strain energy between different processes during earthquake rupture remains a long-standing and fundamental issue in seismology (see *Kanamori and Heaton* [2000] and references therein). The discrepancy between laboratory-based predictions and field measurements of surface heat flow [e.g., *Brune et al.*, 1967; *Lachenbruch and Sass*, 1980] motivates the development of a quantitative approach to partitioning dissipated energy in sheared amorphous materials on both the laboratory scale and the seismic scale.

[3] In this paper, we present a physical model of energy dissipation in a sheared layer of granular fault gouge. The behavior of the gouge layer is described by shear transformation zone (STZ) theory, a continuum model of plastic deformation in amorphous solids that quantifies local configurational disorder and resolves spontaneous localization of strain [*Falk and Langer*, 1998]. Strain localization has been observed in numerical simulations [*Morgan and Boettcher*, 1999], laboratory experiments [*Marone*, 1998], and field studies [*Chester and Chester*, 1998].

[4] Two key features of the STZ description play a role in energy dissipation. First, strain localization leads to rapid weakening and reduces the dynamic sliding stress, thereby decreasing the total energy dissipated. Second, a fraction of the total energy is dissipated to increasing local configurational disorder. In this study, we quantify configurational energy and attribute the remaining dissipated energy to thermal heating assuming fixed material properties.

[5] The primary result of this paper is the STZ energy partition shown in Figures 1b and 1c in the absence and presence of strain localization, respectively. We determine the shear stress s as a function of slip u and calculate the total energy dissipated per unit area, given by $\int s(u)\,du$. This is partitioned between configurational and thermal energy per area, indicated respectively by the hatched and shaded regions in Figures 1b and 1c.

[6] Traditionally, $s(u)$ is estimated using constitutive friction laws such as slip-weakening [*Ida*, 1972; *Andrews*, 1976a, 1976b] or rate- and state-dependent laws [*Dieterich*, 1979; *Ruina*, 1980]. As a coarse approximation, the total heat dissipated per unit area is $s_F\,u_T$, where s_F is the dynamic sliding stress and u_T is the total slip. The remaining dissipated energy is attributed to rock fracture [*Kanamori and Heaton*, 2000]. For the remainder of this paper, we refer to this as the heuristic energy partition. The heuristic partition can applied to any friction law, but for illustrative purposes, we apply it to the STZ friction law in the absence of localization. This is shown in Figure 1a, where the thermal and fracture energy dissipated per unit area are indicated respectively by the shaded and cross-hatched regions. The heuristic partition is also indicated by horizontal dotted lines in Figures 1b and 1c. Compared to the heuristic estimate, the STZ friction law dissipates less thermal heat both in the presence and in the absence of localization. The results presented here do not alone fully resolve the discrepancy between predicted and measured seismic heat flow, especially for large earthquakes. Rather, the main purpose of this paper is to define a concrete pathway for systematic evaluation of the energy flows during earthquakes based on the underlying, nonequilibrium statistical physics. Only relatively simple processes associated with local, nonaffine rearrangements during plastic deformation are included in the current STZ model for fault gouge, but already the net effect of these local processes significantly reduces the estimated thermal heating compared to tradi-

[1]Department of Physics, University of California, Santa Barbara, California, USA.
[2]Geophysics Group and Center for Nonlinear Studies, Los Alamos National Laboratory, Los Alamos, New Mexico, USA.

0148-0227/10/2009JB006960

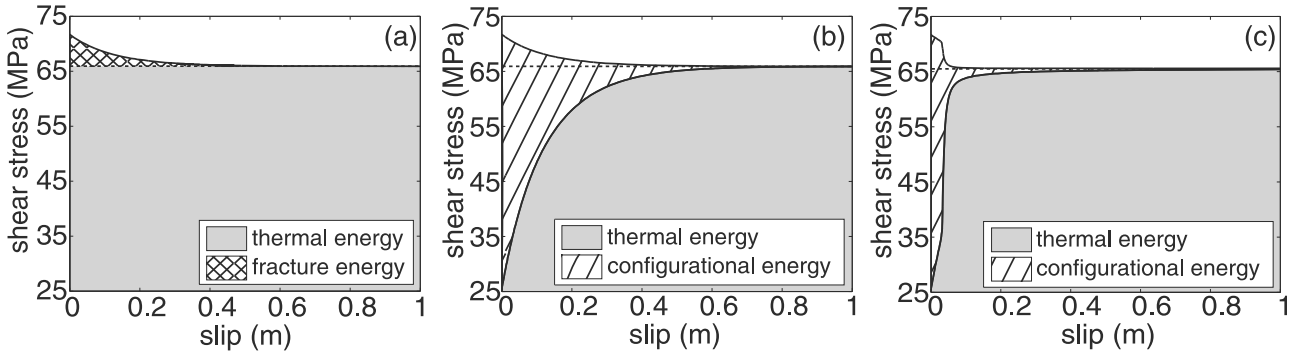

Figure 1. Partition of dissipated energy using (a) heuristic partitioning, (b) STZ partitioning for homogeneous deformation, and (c) STZ partitioning for strain-localized deformation. The total energy dissipated per unit area, indicated by the total filled region in Figures 1a–1c, is less in the strain-localized system than in the homogeneous system. Dissipated energy is partitioned between thermal energy (heat) and configurational energy (local disorder), indicated respectively by the shaded and hatched regions. During the initial stress drop, a large fraction of energy is dissipated to increasing local disorder. As the stress stabilizes, the local disorder approaches its steady-state value, and all energy is dissipated as heat. The heuristic partition shown in Figure 1a is also indicated by the horizontal dotted lines in Figures 1b and 1c. Dissipated energy is partitioned between a coarse estimate of the thermal energy and the fracture energy, indicated respectively by the shaded and cross-hatched regions. Note that the total heat dissipated per unit area, indicated by the total shaded region in Figures 1a–1c, is less in both the homogeneous and strain-localized systems than predicted using the heuristic partition.

tional methods. In future studies, the STZ model may be generalized to include additional physical mechanisms, such as grain fracture and thermally varying material properties, which we expect will lead to further reductions.

[7] The remainder of this paper is organized as follows. In section 2, we review STZ theory within the context of a simple slider model of sheared granular material. We follow in section 3 by calculating shear stress as a function of slip in the presence and absence of strain localization. In section 4, we quantify the partition of dissipated energy between configurational and thermal energy and calculate the total heat dissipated per unit area for several values of poorly constrained parameters. We conclude in section 5 by discussing potential applications of this model and additional considerations for quantifying energy dissipation.

2. Model

[8] We model seismic slip by considering a sheared layer of granular material driven at the boundaries at a fixed velocity V_0. We choose a coordinate system in which the shear stress is applied in the x direction and the width of the layer is resolved in the z direction. We assume that the shear stress is uniform in all directions and that the plastic strain rate $\dot{\gamma}_{pl}$ varies only across the gouge width. We consider a one-dimensional cross section of the gouge layer and resolve $\dot{\gamma}_{pl}$ on a spatial grid that spans the width. Figure 2 shows a schematic of the model.

[9] The dynamics of the granular layer are governed by STZ theory, which has been used to describe a variety of amorphous systems such as glassy materials [*Falk and Langer*, 1998, 2000; *Manning et al.*, 2007, 2009], thin film lubricants [*Lemaitre and Carlson*, 2004], granular flow [*Lois et al.*, 2005], and granular fault gouge [*Daub and Carlson*, 2008; *Daub et al.*, 2008]. This description connects the properties of the granular layer across a range of different length and time scales and is suitable for describing both geophysical and laboratory systems.

[10] Amorphous materials are composed of particles which can move and rearrange in response to applied stress. When sheared, the response of an amorphous material can be approximated by two independent components; affine motion, in which particle displacements are homogeneous, and nonaffine motion, in which particle displacements are inhomogeneous. Simulations of sheared amorphous mate-

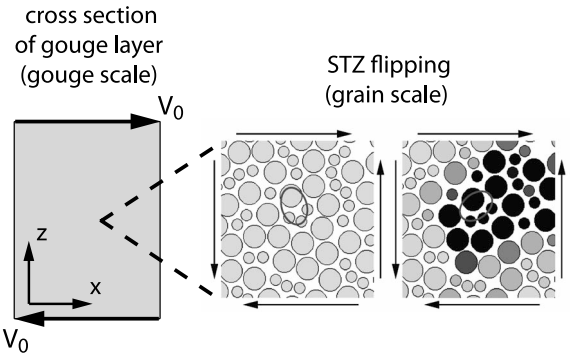

Figure 2. Schematic diagram of sheared granular material at the gouge scale and the grain scale. (left) At the gouge scale, a granular layer is driven at the boundaries at constant velocity V_0. (right) At the grain scale, localized regions undergo configurational rearrangements under applied shear stress. An oval marks the orientation of a region (STZ) in which individual grains switch nearest neighbor contacts. As the material is sheared, the orientation of the STZ aligns with the direction of maximum principal stress. STZ figure reprinted with permission from [*Falk and Langer*, 1998], copyright 1998 by the American Physical Society.

Table 1. Definitions of Functions $R(s)$ and $\hat{\chi}(\dot{\gamma}_{pl})$ and Descriptions of Integration Parameters Used in Equations (1)–(3)

Functions $R(s) = (1 - s_y/s)\exp(-f_0 + s/s_c\chi)$ $\hat{\chi}(\dot{\gamma}_{pl}) = A/\log(q_0/\tau_0\dot{\gamma}_{pl})$	
Parameter	Description
$c_0 = 10$	specific heat
$\epsilon_0 = 10$	average number of grains in an STZ
$\tau_0 = 10^{-6}$ s	timescale of STZ flip
$q_0 = 0.08$	strain at which χ diverges
$s_y = 50$ MPa	yield stress
$s_c = 75$ MPa	STZ stress scale
$f_0 = 1$	STZ activation barrier
$A = 0.1$	rate parameter
$D = 10^{-2}$ m^2	squared diffusion length scale
$\mu = 30$ GPa	shear modulus

rials reveal that nonaffine motion is accommodated in localized regions, called shear transformation zones (STZs), which undergo configurational rearrangement under applied shear stress [*Falk and Langer*, 1998, 2000]. The average STZ constitutes approximately $\epsilon_0 = 10$ particles, and particle rearrangements align the orientation of the STZ with the direction of maximum principal stress.

[11] STZs are modeled as localized regions that flip between two bistable orientations, anti-aligned and aligned, under applied shear stress. An example of this behavior is shown in Figure 2, where the STZ (indicated by the oval outline) flips from an anti-aligned to an aligned orientation as the individual particles rearrange. A single STZ flipping event generates a fixed amount of local plastic strain within the material, and macroscopic plastic strain is the cumulative result of many local events.

[12] Once flipped, STZs cannot further deform, and thus they are continually created and destroyed in order to further accommodate plastic strain within the material. This drives the STZ density toward a Boltzmann distribution $\exp(-1/\chi)$ [*Langer*, 2008; *Langer and Manning*, 2008] with a dimensionless effective disorder temperature χ. The effective temperature is a continuum field that characterizes the amount of configurational disorder in the system.

[13] Thermal fluctuations are not sufficient to drive STZ reversal at the granular scale, and therefore the rate at which STZs flip orientations, given by the rate-switching function $R(s) = f(s)(1 - s_y/s)\exp(s/s_c\chi)$, depends only on the shear stress s and the effective temperature χ. The form of $R(s)$ is imposed by physical constraints which require that $f(s)$ be a symmetric function of s [*Bouchbinder and Langer*, 2009]. Although different materials are governed by different forms, similar behavior is observed regardless of the specific choice of $f(s)$. We choose $f(s) = \exp(-f_0)$, where f_0 is the STZ activation energy scaled by the STZ formation energy and is analogous to the reference friction coefficient in the Dieterich-Ruina friction law. The parameters s_y and s_c are the yield stress and the STZ formation stress, respectively, where s_c is the largest stress scale in the system.

[14] The plastic strain rate $\dot{\gamma}_{pl}$ depends on both the STZ density $\exp(-1/\chi)$ and the rate of flipping $R(s)$:

$$\dot{\gamma}_{pl} = (\epsilon_0/\tau_0)R(s)\exp(-1/\chi). \tag{1}$$

The shear stress and the effective temperature evolve according to the following equations:

$$\frac{\partial s}{\partial t} = \frac{\mu}{w}\left(V_0 - \int_{-w}^{w}\dot{\gamma}_{pl}\,dz\right); \tag{2}$$

$$\frac{\partial \chi}{\partial t} = \frac{\dot{\gamma}_{pl}s}{c_0 s_y}\left(1 - \frac{\chi}{\hat{\chi}(\dot{\gamma}_{pl})}\right) + \frac{\partial}{\partial z}\left(\dot{\gamma}_{pl}D\frac{\partial \chi}{\partial z}\right). \tag{3}$$

The parameters in equations (1)–(3) are described in Table 1.

[15] The first and second terms on the right-hand side of equation (2) describe the competing effects of elastic and plastic deformation, respectively. The first term on the right-hand side of equation (3) describes energy dissipated to increasing χ as it is driven toward the steady-state value $\hat{\chi}(\dot{\gamma}_{pl})$ [*Langer and Manning*, 2008]. The specific heat c_0 determines the amount of energy required to increase the effective temperature. The second term describes the diffusion of χ across the width of the gouge layer, a property observed in simulations of amorphous materials [*Shi et al.*, 2007]. The diffusion rate is determined in part by the diffusion length scale $\sqrt{D}$, which is on the order of the characteristic grain size of the material.

[16] The form of $\hat{\chi}(\dot{\gamma}_{pl}) = A/\log(q_0/\tau_0\dot{\gamma}_{pl})$ is taken from steady-state simulations of glassy materials [*Langer and Manning*, 2008]. $\hat{\chi}(\dot{\gamma}_{pl})$ depends explicitly on the strain $q = \tau_0\dot{\gamma}_{pl}$, where τ_0 is the timescale of STZ flipping. For granular materials, the value of τ_0 is estimated to be the average grain size divided by the speed of sound in the material. Simulations reveal that the effective temperature diverges at a finite strain q_0. From molecular dynamics simulations, this value is estimated to be 0.08 [*Haxton and Liu*, 2007]. For geophysical materials, we can alternatively find a value for q_0 by estimating the strain rate at which the material transitions from quasi-static to inertial granular flow. This transition can be characterized by the inertial number of the material, which compares a collisional timescale to a deformation timescale and scales with the ratio of the strain rate to the square root of the normal stress [*Jop et al.*, 2006]. For pressures at seismogenic depth, an inertial number of 1 gives a strain rate on the order of 5×10^6. This value corresponds to a dimensionless strain $q_0 = 5$, which far exceeds the molecular dynamics estimate of 0.08. We therefore take $q_0 = 0.08$ as a conservative estimate. For strain rates exceeding q_0/τ_0, the system exhibits amorphous flow rather than localized deformation and is no longer governed by STZ theory. Because τ_0 is the fastest timescale in the system, the value of q_0/τ_0 at which this occurs exceeds the strain rates typically attained during seismic slip.

[17] The rate parameter A determines whether the stress increases (rate strengthening) or decreases (rate weakening) with increasing strain rate. For a given set of parameters, there is a critical value A_{crit} which separates the rate-weakening regime ($A < A_{\mathrm{crit}}$) from the rate-strengthening regime ($A > A_{\mathrm{crit}}$). For seismic stresses, A_{crit} is approximately less than unity, but the specific value of A_{crit} depends on the parameters within $R(s)$ and $\hat{\chi}(\dot{\gamma}_{pl})$ in a complicated manner. The STZ stress scale s_c is the least constrained of these parameters, and, in general, A_{crit} increases with increasing values of s_c. Previous studies have shown that steady sliding is

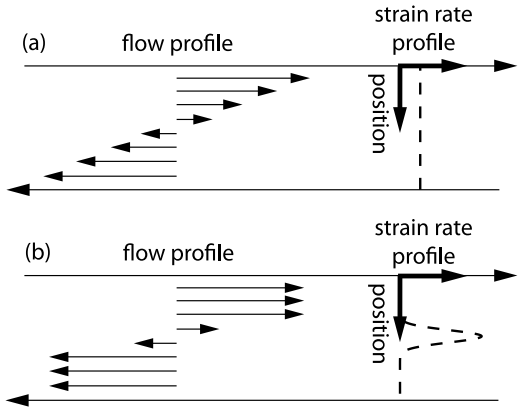

Figure 3. Flow and strain rate profiles for (a) homogeneous deformation and (b) strain-localized deformation in a layer of sheared amorphous material. In Figure 3a, a uniform initial effective temperature profile results in homogeneous deformation. The flow gradually transitions across the layer, and the strain rate profile is uniform. In Figure 3b, inhomogeneities in the initial effective temperature profile provide a mechanism for strain localization. Large regions of the material flow with the boundaries, while a localized region exhibits an abrupt change in flow. This is accompanied by a sharp peak in the strain rate profile. While the localization shown here is centered within the gouge layer, asymmetric effective temperature perturbations result in off-center localization.

unstable to perturbations in effective temperature for rate-weakening parameters [*Manning et al.*, 2009]. Transient effects can also lead to instabilities for rate-strengthening parameters [*Manning et al.*, 2009].

[18] We use rate-weakening parameters and consider both homogeneous and strain-localized deformation, shown diagrammatically in Figure 3. A homogeneous effective temperature profile results in the laminar flow and uniform plastic strain rate shown in Figure 3a. Perfectly homogeneous effective temperature conditions correspond to perfect uniformity in the material, which is physically unrealistic. However, homogeneous flow profiles arise in certain parameter regimes (e.g., when the diffusion length scale is large compared to the width of an interfacial layer) and are appropriate for describing friction specified at an interface. More realistic conditions exhibit inhomogeneities in effective temperature, which provide a mechanism for strain localization. Regions of higher effective temperature have a higher STZ density and a larger strain rate, and therefore the effective temperature increases more rapidly in these regions. This results in the localization shown in Figure 3b, which is indicated by an abrupt change in flow and a peak in strain rate.

3. Dynamics

[19] To study the dynamics of the sheared gouge layer, we numerically integrate equations (2) and (3) using a finite difference method with an adaptive time step. We consider a gouge layer with shear modulus $\mu = 30$ GPa and half-width $w = 1$ m driven at the boundaries at velocity $V_0 = 1$ m/s for an initial shear stress of 70 MPa.

[20] Integration parameters are defined in Table 1. Parameter values were chosen to obtain rate-weakening behavior at stress and strain rate values suitable for describing seismic slip. The dynamics are qualitatively similar regardless of the specific parameter values. However, variations in the parameters s_c, A, D, and c_0 give rise to the largest quantitative change in the dynamics. The effect of varying these parameters will be discussed in the latter portion of this section.

[21] We consider the two separate cases of homogeneous and inhomogeneous initial effective temperature profiles. In the first case, we choose $\chi(t = 0) = 0.003$. The same behavior is observed regardless of the specific choice of $\chi(t = 0)$, although decreasing the value increases the peak shear stress required to initiate slip (e.g., for $\chi(t = 0) = 0.002$, $s_{\text{peak}} \sim 73$ MPa). By symmetry, χ and $\dot{\gamma}_{pl}$ remain homogeneous across the gouge width for the duration of the simulation. In the second case, we introduce a small initial effective temperature perturbation in the middle of the layer, $\chi(t = 0) = 0.003 + 0.00001/[\exp(10x) + \exp(-10x)]$. As a single shear-band forms at the location of the largest initial perturbation regardless of the complexity of the inhomogeneous initial conditions [*Manning et al.*, 2007], a perturbation centered within the gouge layer reproduces the dynamics of general heterogeneous conditions.

[22] As the material is sheared, the slip u increases with time at a constant rate of 2 V_0. The evolution of the shear stress $s(u)$ is shown in Figure 4 for both cases. In the homogeneous case, the stress slowly decreases to a steady-state dynamic sliding stress s_f of approximately 65.9 MPa, exhibiting logarithmic weakening behavior similar to that seen using the Dieterich-Ruina constitutive friction law [*Dieterich*, 1979]. In the strain-localized case, the stress dependence matches that of the homogeneous system for small values of slip. As slip increases, a shear-band forms and the stress rapidly decreases. Following the formation of the shear-band, the strain-localized system stabilizes more quickly and reaches a lower dynamic sliding stress (~65.6 MPa) than does the homogeneous system.

[23] In both systems, the net stress drop Δs is small (~6 MPa) relative to the total stress. The stress drop is controlled by the parameters s_c and A and by the form of the rate-switching function $R(s)$. Based on physical considerations, the STZ stress scale s_c must be greater than the yield stress s_y [*Bouchbinder and Langer*, 2009]. As $s_c/s_y \rightarrow 1$, the strain rate exceeds the value within which STZ theory is valid, and the system melts. Increasing the value of s_c/s_y increases the net stress drop but also increases the dynamic sliding stress in both systems (e.g., for $s_c/s_y = 2$, $\Delta s \sim 9$ MPa and $s_f \sim 87$ MPa). For this study, we chose the smallest value of s_c/s_y for which the system did not melt. The rate parameter A influences the extent of weakening in the material. Increasing the value of A increases the net stress drop in both systems, but the stress requires a greater amount of slip to stabilize. For this study, we chose the largest value of A within the rate-weakening regime for which the stress in both the homogeneous and strain-localized systems stabilized within a total slip of 1 m. Last, various choices for the form of symmetric function $f(s)$ within $R(s)$ may be appropriate for describing other sys-

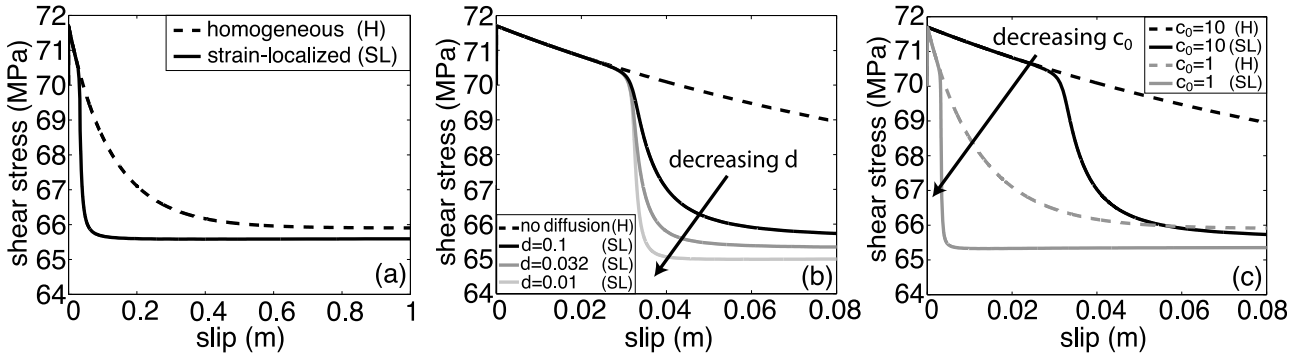

Figure 4. Figure 4a shows shear stress as a function of slip for homogeneous (H) and strain-localized (SL) deformation. Parameter values are varied in Figures 4b and 4c, with the black curves indicating the stress dependence shown in Figure 4a. Homogeneous deformation is characterized by a uniform initial effective temperature profile, and the stress weakens logarithmically. Inhomogeneities in effective temperature provide a mechanism for shear-band formation. As a result, the SL system exhibits rapid weakening following the formation of a shear-band, and the stress stabilizes at lower value than in the H system. Figure 4b shows the stress dependence for decreasing values of $d = \sqrt{D}/w$, the ratio of the diffusion length scale to the gouge half-width. A shear-band forms at the same value of slip regardless of the value of d. As d decreases, the stress decreases more rapidly following the formation of the shear-band, and the system stabilizes at a lower dynamic sliding stress. The evolution of the H system, for which there is no diffusion, is indicated for comparison. Figure 4c shows the stress dependence for two values of the specific heat c_0. Decreasing the value of c_0 decreases the slip over which the stress evolves. In addition, it decreases the value of the dynamic sliding stress achieved by the SL system. The H system stabilizes at the same dynamic sliding stress regardless of the value of c_0.

tems and could yield larger net stress drops. For example, previous studies have used a power law form for $R(s)$ to describe the dynamics of glassy materials [*Langer and Manning*, 2008]. However, in order for a granular gouge layer to undergo plastic deformation, a power law form of $R(s)$ requires that the stress far exceed the value which can be withstood by crustal material. Such a form is therefore not suitable for describing seismic slip. Of the parameters listed in Table 1, the diffusion length scale $\sqrt{D}$ and the specific heat c_0 are the least constrained. Figures 4b and 4c show the stress dependence for both homogeneous and strain-localized deformation using several values of $\sqrt{D}$ and c_0.

[24] The diffusion length scaled by the gouge half-width, $d = \sqrt{D}/w$, determines the width of the shear-band formed in the strain-localized system. When $d \rightarrow 1$, the shear-band fills the width of the gouge layer. Decreasing the value of d results in a narrower shear-band. The shear-band forms at the same value of slip regardless of the value of d, but the stress decreases more rapidly and stabilizes at a lower value for smaller values of d. Deformation does not occur over a length scale smaller than the grain size, so this places a lower bound on the value of d. The strain-localized stress dependence is shown in Figure 4b for decreasing values of d. The homogeneous system is unaffected by the value of d.

[25] The specific heat c_0 affects how quickly the stress stabilizes. For smaller values of c_0, both the effective temperature and the stress evolve more rapidly, and the system stabilizes at a smaller value of slip. In addition, decreasing the value of c_0 decreases the width of the shear-band formed in the strain-localized system. As a result, while the homogeneous system stabilizes at the same dynamic sliding stress regardless of the value of c_0, the strain-localized system stabilizes at a lower dynamic sliding stress for smaller values of c_0. This is shown in Figure 4c for two values of c_0.

4. Energy Budget

[26] As the gouge layer is sheared, energy is required to change the effective temperature and increase local disorder. The total change in effective temperature as a function of slip, $\int (\partial\chi/\partial u)\, dz$, is a sum over all incremental changes $\partial\chi/\partial u$ across the gouge width. These changes require a configurational energy per unit area $c_0 s_y \int \int (\partial\chi/\partial u)\, dz\, du$, where $c_0 s_y$ sets the energy scale of the configurational system.

[27] We attribute the remaining dissipated energy to thermal heating. The heat dissipated per unit area is the difference between the total and configurational energy dissipated per unit area, $\int [s(u) - c_0 s_y \int (\partial\chi/\partial u)\, dz]\, du$. We assume that material properties do not vary as heat is dissipated into the system. Although not treated in this study, we expect that thermally varying material properties would further contribute to weakening, and we discuss future work in this direction in section 5.

[28] The partition between these two energy sinks is shown in Figures 1b and 1c for homogeneous and strain-localized deformation, respectively. The stress curves shown in Figure 4a are the upper bounding curves in Figures 1a–1c. The total energy dissipated per unit area, $\int s(u)\, du$, is indicated by the total filled region beneath each of these curves. By comparing the total filled regions in Figures 1b and 1c, we can immediately see that strain localization decreases the total energy dissipated per unit area. This results from the rapid decrease in stress and the lower dynamic sliding stress that characterizes strain-localized dynamics. However, as the net stress drop is small

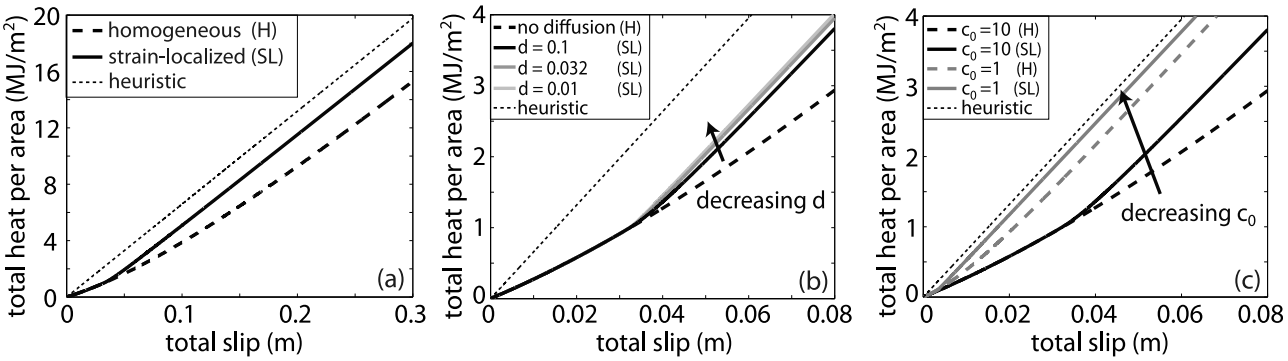

Figure 5. Figure 5a shows total heat dissipated per unit area as a function of total slip u_T for homogeneous (H) and strain-localized (SL) deformation compared to the heuristic estimate. Parameter values are varied in Figures 5b and 5c, with the black curves indicating the dependence shown in Figure 5a. For small values of u_T, both systems dissipate the same amount of heat. As u_T increases, a shear-band forms in the SL system, resulting in more heat dissipation due to a rapid equilibration of the effective temperature and an increased rate of heat production. For large values of u_T, the rate of heat production, indicated by the slope of each curve, is constant in both systems but is lower in the SL system. Figure 5b shows this dependence for decreasing values of $d = \sqrt{D}/w$. The value of d does not affect the value of u_T at which the H and SL curves separate. For a given value of u_T beyond this point, decreasing d increases the total heat dissipated and decreases the long-term rate of heat production in the SL system. Figure 5c shows this dependence for two values of c_0. For the smaller value of c_0, both the H and SL systems dissipate more heat for a given value of u_T. In addition, a shear-band forms more quickly in the SL system, resulting in a rapid increase in heat production at a smaller value of u_T. While the long-term rate of heat production in the homogeneous system is unaffected by the choice of c_0, decreasing the value of c_0 decreases the long-term rate of heat production in strain-localized systems. In all cases, the total heat dissipated in each system is less than the heuristic value, which is indicated by the dotted curve.

in both cases, the total energy dissipated per unit area is large compared to the change due to strain localization.

[29] The thermal and configurational energy dissipated per unit area are indicated respectively by the shaded and hatched regions in Figures 1b and 1c. The heat dissipated per unit volume, $s(u) - c_0 s_y \int (\partial\chi/\partial u)\, dz$, defines the boundary between these two regions. During the initial stress drop, the effective temperature is increasing rapidly. This process requires a large fraction of the total energy, leaving only a small fraction to be dissipated as heat. As the stress stabilizes, the effective temperature approaches its steady-state value $\hat{\chi}(\dot{\gamma}_{pl})$. In steady state, no additional energy is dissipated to increasing local disorder, and all energy is dissipated as heat. This can be seen in Figures 1b and 1c when the boundary between regions approaches the constant dynamic sliding stress in both systems.

[30] For comparison, the heuristic partition between heat and fracture energy is shown in Figure 1a assuming the homogeneous stress dependence shown in Figure 1b. The fracture and thermal energy dissipated per unit area are indicated by the cross-hatched and shaded regions, respectively. When we compare the size of the shaded regions in Figures 1a, 1b, and 1c, we see that less heat is dissipated per unit area in both the homogeneous and strain-localized systems than predicted by the heuristic estimate.

[31] Once the effective temperature reaches steady state, increasing slip only dissipates more heat into the system. The total slip, which varies in both geophysical and laboratory systems, determines the fraction of energy dissipated as heat. In order to discuss this dependence, we calculate the total heat dissipated per unit area as a function of total slip u_T for all three systems shown in Figure 1. This is found by calculating the total area of each shaded region for increasing values of u_T. The results are shown in Figure 5a.

[32] For small values of u_T, a shear-band has not yet formed in the strain-localized system. As a result, both the homogeneous and strain-localized systems show the same stress dependence and dissipate the same amount of total heat.

[33] For $u_T \gtrsim 0.03$ m, a shear-band has formed in the strain-localized system, marking the separation between the homogeneous and strain-localized curves shown in Figure 5a. Both the shear stress and the effective temperature stabilize more quickly following the formation of a shear-band, at which point no additional energy is dissipated to increasing local disorder. This results in a rapid increase in heat production, as energy not dissipated to increasing local disorder must be dissipated as heat. This is illustrated in Figure 1, where the boundary between shaded regions increases more quickly in the strain-localized system than in the homogeneous system. This is also shown in Figure 5, where the slope of the strain-localized curve increases more rapidly than the slope of the homogeneous curve for $u_T \gtrsim 0.03$ m. As a result, the strain-localized system dissipates more total heat per unit area than the homogeneous system for $u_T \gtrsim 0.03$ m.

[34] For large values of u_T, both the stress and the effective temperature have stabilized. In steady state, all energy is dissipated as heat, and the long-term rate of heat production is constant. This is true of all three systems and can

be seen in Figure 1 when the boundary between shaded regions matches the constant dynamic sliding stress in Figures 1a–1c. The strain-localized system stabilizes at a lower dynamic sliding stress and therefore has a lower long-term rate of heat production than the homogeneous system. Although not detectable in Figure 5a, the strain-localized curve has a slightly smaller slope than the homogeneous curve for large values of u_T. As a result, the homogeneous system dissipates more total heat per unit area than the strain-localized system for $u_T \gtrsim 10$ m, a regime which may be relevant for describing local slip events during large earthquakes.

[35] The rate of heat production in both the homogeneous and strain-localized systems is less than or equal to that obtained using the heuristic partition. As a result, the total heat dissipated in each system is less than the heuristic estimate. If the initial effective temperature is sufficiently small, there can be a short-lived transient phase during which the heuristic estimate may lie below that of the STZ model for both homogeneous and strain-localized deformation. In our simulations, this effect occurs for extremely small values of slip ($\lesssim 10^{-5}$ m) and is not visible in Figures 1 and 5. In the absence of infinitely stiff boundary conditions, the short-lived transient behavior is confined to the creep phase that precedes unstable sliding. Figures 5b and 5c show the total heat dissipated per unit area for different values of $d = \sqrt{D}/w$ and c_0, respectively. These results are found using the stress curves shown in Figures 4b and 4c.

[36] The value of d affects the rate of heat production in the strain-localized system for $u_T \gtrsim 0.03$ m. As d decreases, the stress and the effective temperature stabilize more rapidly, and the stress stabilizes at a lower dynamic value. As a result, the heat production increases more rapidly but approaches a lower long-term rate. This is shown in Figure 5b, where the total heat curve of the strain-localized system separates more rapidly from the homogeneous curve for smaller values of d. As a result of this separation, strain-localized systems with smaller values of d dissipate more total heat per unit area for $u_T \gtrsim 0.03$ m. Although not detectable in Figure 5b, decreasing the value of d also decreases the slope of the strain-localized curves for large values of u_T. In this regime, systems with larger values of d, for which the long-term rate of heat production is higher, dissipate more total heat per unit area.

[37] The value of c_0 affects the rate of heat production in both the homogeneous and strain-localized systems. Systems with smaller values of c_0 require less energy to change the effective temperature. As c_0 decreases, the effective temperature stabilizes more rapidly in both systems, resulting in a more rapid increase in heat production. This is shown in Figure 5c, where the slopes of both the homogeneous and strain-localized curves increase more rapidly for $c_0 = 1$ than for $c_0 = 10$. As a result, both systems dissipate more heat per unit area for smaller values of c_0. In addition, a shear-band forms more rapidly in the strain-localized system for smaller values of c_0. This is shown in Figure 5c when the strain-localized curve separates from the homogeneous curve at a smaller value of total slip for $c_0 = 1$ than for $c_0 = 10$. Last, decreasing the value of c_0 decreases the dynamic sliding stress attained by the strain-localized system, resulting in a lower long-term rate of heat production. Although not detectable in Figure 5c, the slope of the strain-localized curve is smaller for $c_0 = 1$ than for $c_0 = 10$ for large values of u_T. In this regime, strain-localized systems with larger values of c_0, for which the long-term rate of heat production is higher, dissipate more total heat per unit area. In contrast, the long-term rate of heat production in homogeneous systems is unaffected by changes in c_0.

[38] While the strain-localized system alone is sensitive to changes in $\sqrt{D}$, both systems are sensitive to changes in c_0. In addition, both systems are more sensitive to changes in c_0 than to changes in $\sqrt{D}$ of the same order of magnitude. This is indicated by the larger variation in total heat production per unit area seen in Figure 5c as compared to Figure 5b. Although neither $\sqrt{D}$ nor c_0 is well constrained, these results indicate that changes in c_0 are more significant for the study of heat dissipation.

5. Discussion

[39] These results indicate that changes in local configurational disorder play a significant role in energy dissipation within sheared amorphous materials. Not only do they provide a mechanism for strain localization, they also dissipate energy that is traditionally attributed to heating and fracture. While the simple slider model presented here focuses on dissipation, dynamic rupture simulations could be used to quantify additional radiated energy. With good estimates of total slip, this description produces a similar stress dependence to that found using a full dynamic rupture simulation of the STZ equations [*Daub et al.*, 2008] and therefore should show a similar partition between thermal and configurational energy.

[40] We find that the rate of heat dissipation, and thus the change in temperature of the gouge material, increases as a function of slip and approaches a constant, steady-state value. The homogeneous system shows a gradual increase in the rate of heat production that stabilizes at large value of slip. In contrast, the strain-localized system shows a more rapid increase in the rate of heat production that approaches a similar steady-state value but stabilizes at a smaller value of slip. This indicates that the measured change in temperature of the material should grow more gradually in homogeneous materials than in inhomogeneous materials. This prediction agrees with recent heat emission measurements taken on a halite slider in the absence and presence of granular gouge material [*Mair et al.*, 2006], which can be modeled as homogeneous and inhomogeneous STZ systems, respectively. It was found that the rise in temperature increased more rapidly in the presence of gouge material, but both systems approached similar steady-state values. In addition, the rate of temperature change was found to increase in both systems with increasing velocity, indicating rate-strengthening behavior. While the present work focuses on rate-weakening dynamics, the STZ description can be used to describe the rate-strengthening regime and should give rise to a velocity dependence similar to that observed by *Mair et al.* [2006]. In the future, we plan to directly test the agreement of our model with these measurements by quantifying heat dissipation in the rate-strengthening regime. In addition, laboratory slider experiments are useful for studying rate-weakening behavior in granular materials and could test the predictions shown in this paper.

[41] When compared to heuristic descriptions of energy dissipation, we find that both the homogeneous and strain-localized systems dissipate less total heat. While the deviation from the heuristic estimate is approximately 3.5% in the strain-localized system and approximately 7.5% in the homogeneous system for a total slip of 1 m, it is as large as 58% in both systems for small values of total slip (~0.01 m). The STZ description quantifies the contribution of two distinct processes to the reduction in heat dissipation. First, strain localization decreases the total dissipated energy, and second, configurational rearrangements dissipate a fraction of this total energy, thereby decreasing the fraction dissipated as heat. For large values of slip, this reduction is not sufficient to explain the lack of a measured heat flow anomaly. However, we expect that additional mechanisms, such as thermal weakening and fracture, will further contribute to a reduction in heat flow.

[42] As thermal heating is not treated in detail here, a more complete treatment is likely to show additional weakening effects due to variations in material properties with increasing temperature. Thermal effects, such as fluid pressurization [*Lachenbruch*, 1980], flash heating [*Tullis and Goldsby*, 2003], and frictional melting [*Di Toro et al.*, 2006], have all been shown to contribute to thermal weakening. However, studies suggest that these processes require localized deformation (see *Rice* [2006] and references therein). The STZ model provides a method for explicitly determining the extent of strain, and thus thermal heat, localization within the gouge layer. We expect that material properties such as the shear modulus μ, the yield stress s_y, the activation energy f_0, and the STZ stress scale s_c will vary with increasing heat dissipation. The evolution of these parameters will depend not only on the slip but also on the extent of localization. Thermal weakening of the gouge material could affect the rate of STZ reversal and the evolution of the effective temperature, and we expect this to result in an additional decrease in shear stress as a function of slip.

[43] Additional mechanisms not treated here may also contribute to energy dissipation. Fracture of individual grains could alter the grain size distribution and could affect the STZ timescale τ_0 and the diffusion length scale $\sqrt{D}$. A varying value of $\sqrt{D}$ would affect the rate at which the stress weakens and the dynamical value of the stress. In addition, the average grain size size is expected to decrease as a function of slip. Treatment of this effect could involve modeling the STZ formation energy as a dynamic variable that evolves as the material is sheared. This is expected to alter the rate of STZ reversal, thereby altering the stress dependence.

[44] When scaling this model to laboratory systems, both the relevant length scales and stress scales change. While the gouge layer along a fault may be up to several meters thick, the thickness of laboratory layers is often on the order of millimeters. In addition, the value of $\sqrt{D}$ scales with the characteristic grain size, which depends on the structure of the material. However, the grain size distribution varies greatly in both fault and laboratory systems, and the dependence of $\sqrt{D}$ on grain size distribution is not yet understood. The stress parameters s_y and s_c and the shear stress s scale with the normal stress, and we expect that the other STZ parameters will have similar values to those used in this study. As a result, laboratory systems should exhibit similar qualitative behavior to the results shown here.

[45] For large values of total slip, the total heat dissipated per unit area is greatly influenced by the dynamic sliding stress, determined in part by the rate-switching function $R(s)$. Different forms of the symmetric function $f(s)$, which may be appropriate for describing other systems, will affect the amount of energy dissipated as heat. While our choices for $R(s)$ reflect the properties of granular fault gouge, appropriate choices can be made to describe laboratory systems such as lubricated boundaries or granular flows. As strain localization occurs regardless of the specific form of $R(s)$, the effect of rapid weakening on energy dissipation can be studied within the context of a variety of other geophysical and laboratory systems.

[46] **Acknowledgments.** The authors thank James Langer and Ralph Archuleta for useful discussions. This work was supported by the Department of Education, CFDA number 84.200, the David and Lucile Packard Foundation, NSF grant number DMR-0606092, and the NSF/USGS Southern California Earthquake Center, funded by NSF Cooperative Agreement EAR-0529922 and USGS Cooperative Agreement 07HQAG0008. The SCEC contribution number for this paper is 1328.

References

Andrews, D. J. (1976a), Rupture propagation with finite stress in antiplane strain, *J. Geophys. Res.*, *81*(20), 3575–3582.

Andrews, D. J. (1976b), Rupture velocity of plane strain shear cracks, *J. Geophys. Res.*, *81*(32), 5679–5687.

Bouchbinder, E., and J. S. Langer (2009), Nonequilibrium thermodynamics of driven amorphous materials. III. Shear-transformation zone plasticity, *Phys. Rev. E*, *80*, 031133.

Brune, J. N., T. L. Henyey, and R. F. Roy (1967), Heat flow, stress, and rate of slip along the San Andreas Fault, California, *J. Geophys. Res.*, *74*(15), 3821–3827.

Chester, F. M., and J. S. Chester (1998), Ultracataclasite structure and friction processes of the Punchbowl Fault, San Andreas system, California, *Tectonophysics*, *295*, 199–221.

Daub, E. G., and J. M. Carlson (2008), A constitutive model for fault gouge deformation in dynamic rupture simulations, *J. Geophys. Res.*, *113*, B12309, doi:10.1029/2007JB005377.

Daub, E. G., M. L. Manning, and J. M. Carlson (2008), Shear strain localization in elastodynamic rupture simulations, *Geophys. Res. Lett.*, *35*, L12310, doi:10.1029/2008GL033835.

Dieterich, J. H. (1979), Modeling of rock friction 1. Experimental results and constitutive equations, *J. Geophys. Res.*, *84*(B5), 2161–2168.

Di Toro, G., T. Hirose, S. Nielsen, G. Pennacchioni, and T. Shimamoto (2006), Natural and experimental evidence of melt lubrication of faults during earthquakes, *Science*, *311*, 647–649.

Falk, M. L., and J. S. Langer (1998), Dynamics of viscoplastic deformation in amorphous solids, *Phys. Rev. E*, *57*(6), 7192–7205.

Falk, M. L., and J. S. Langer (2000), From simulation to theory in the physics of deformation and fracture, *MRS Bull.*, *25*(5), 40–45.

Haxton, T. K., and A. J. Liu (2007), Activated dynamics and effective temperature in a steady state sheared glass, *Phys. Rev. Lett.*, *99*, 195701.

Ida, Y. (1972), Cohesive force across the tip of a longitudinal-shear crack and Griffith's specific surface energy, *J. Geophys. Res.*, *77*(20), 3796–3805.

Jop, P., Y. Forterre, and O. Pouliquen (2006), A constitutive law for dense granular flows, *Nature*, *441*(8), 727–730.

Kanamori, H., and T. H. Heaton (2000), Microscopic and macroscopic physics of earthquakes, in *Geocomplexity and the Physics of Earthquakes*, American Geophysical Union Geophysical Monograph 120, pp. 147–163, AGU, Washington, D. C.

Lachenbruch, A. H. (1980), Frictional heating, fluid pressure, and the resistance to fault motion, *J. Geophys. Res.*, *85*(B11), 6097–6112.

Lachenbruch, A. H., and J. H. Sass (1980), Heat flow and energetics of the San Andreas Fault zone, *J. Geophys. Res.*, *85*(B11), 6185–6222.

Langer, J. S. (2008), Shear-transformation-zone theory of plastic deformation near the glass transition, *Phys. Rev. E*, *77*, 021502.

Langer, J. S., and M. L. Manning (2008), Steady-state, effective-temperature dynamics in a glassy material, *Phys. Rev. E*, *76*, 056107.

Lemaitre, A., and J. M. Carlson (2004), Boundary lubrication with a glassy interface, *Phys. Rev. E*, *69*(6), 061611.

Lois, G., A. Lemaitre, and J. M. Carlson (2005), Numerical tests of constitutive laws for dense granular flows, *Phys. Rev. E.*, *72*, 051303.

Mair, K., F. Renard, and O. Gunderson (2006), Thermal imaging on simulated faults during frictional sliding, *Geophys. Res. Lett.*, *33*, L19301, doi:10.1029/2006GL027143.

Manning, M. L., J. S. Langer, and J. M. Carlson (2007), Strain localization in a shear transformation zone model for amorphous solids, *Phys. Rev. E*, *76*(5), 056106.

Manning, M. L., E. G. Daub, J. S. Langer, and J. M. Carlson (2009), Rate-dependent shear bands in a shear-transformation-zone model of amorphous solids, *Phys. Rev. E*, *79*, 016110.

Marone, C. (1998), Laboratory-derived friction laws and their application to seismic faulting, *Ann. Rev. Earth Planet. Sci.*, *26*, 643–696.

Morgan, J. K., and M. S. Boettcher (1999), Numerical simulations of granular shear zones using the distinct element method 1. Shear zone kinematics and the micromechanics of localization, *J. Geophys. Res.*, *104*(B2), 2703–2720.

Rice, J. R. (2006), Heating and weakening of faults during earthquake slip, *J. Geophys. Res.*, *111*, B05311, doi:10.1029/2005JB004006.

Ruina, A. L. (1980), Friction laws and instabilities: A quasistatic analysis of some dry frictional behavior, Ph.D. Thesis, Brown University, Providence, RI.

Shi, Y., M. B. Katz, H. Li, and M. L. Falk (2007), Evaluation of the disorder temperature and free-volume formalisms via simulations of shear banding in amorphous solids, *Phys. Rev. Lett.*, *98*, 185505.

Tullis, T. E., and D. L. Goldsby (2003), Flash melting of crustal rocks at almost seismic slip rates, *Eos Trans. AGU*, *84*(46), Fall Meet. Suppl. Abstract S51B-05.

J. M. Carlson and A. M. Hermundstad, Department of Physics, University of California, Broida Hall, Santa Barbara, CA 93106, USA. (ann@physics.ucsb.edu)

E. G. Daub, Geophysics Group and Center for Nonlinear Studies, Los Alamos National Laboratory, Los Alamos, NM 87545, USA.